Computers and Geotechnics 67 (2015) 17–32

Contents lists available at ScienceDirect

Computers and Geotechnics

journal homepage: www.elsevier.com/locate/compgeo

Research Paper

A comparison of finite volume formulations and coupling strategies for two-phase flow in deforming porous media

Roza Asadi *, Behzad Ataie-Ashtiani

Department of Civil Engineering, Sharif University of Technology, PO Box 11155-9313, Tehran, Iran

ARTICLE INFO

Article history:
Received 1 June 2014
Received in revised form 28 January 2015
Accepted 8 February 2015

Keywords:
Finite volume method
Two phase flow
Deformable porous media
Primary variables
Picard scheme
Fully coupled
Iteratively coupled

ABSTRACT

In this paper a locally mass conservative finite volume method is employed to model the one-dimensional, two-phase immiscible flow in a poroelastic media. Since, an appropriate choice of primary variables is critical in simulating multiphase subsurface flow, depending on such a choice, the governing equations can be expressed in different forms. By implementing Picard iteration to a highly nonlinear system of equations, three numerical models including pressure form, mixed form and mixed form with a modified Picard linearization are developed in this study. These models have been evaluated in terms of stability, convergence and mass conservation in various one-dimensional test cases. Selecting water saturation in the mixed form as a primary variable, which is not frequent in the geotechnical engineering, could produce convergence problems in transition from saturated to unsaturated regimes, but in other conditions show good convergence and also mass balance properties. The pressure form and the mixed form with a modified Picard linearization converge in all test cases even near the fully saturated conditions. The pressure form suffers from poor mass balance and the mixed form with a modified Picard linearization poses superior mass balance property than the pressure form. In order to solve the coupled multiphase flow and geomechanics, two coupling strategies are used, first the fully coupled approach and second the iterative algorithm based on the fixed-stress operator split. Comparison between the total number of iterations and the total execution time of the fully coupled method and the fixed-stress schemes are presented through different one-dimensional examples. The accuracy, robustness and efficiency of the fixed-stress method have been demonstrated due to the reduced CPU time and low values of error for different variables.

1. Introduction

The coupling between multiphase flows and geomechanics is of significant interest in a diverse range of engineering fields. In reservoir engineering, examples of applications include land subsidence, hydraulic fracturing, wellbore instability, casing damage and sand production [1]. Within the field of environmental engineering, soil contamination problems caused by the release of petroleum hydrocarbons and immiscible industrial wastes are highly nonlinear and challenging to be solved [2–4] and in some cases they may require a coupled hydro-mechanical analysis in deformable subsystems [5,6]. Moreover, consolidation of partially saturated soils and land settlement due to groundwater pumping are problems of considerable concern in soil mechanics and geotechnical engineering in which coupled simulators are needed [7–11].

To describe multiphase subsurface flow, an appropriate choice of primary variables is critical in simulating the resulting nonlinear system [12,13]. Depending on such a choice, the governing equations can be expressed in different forms. In the context of multiphase flow, the basic formulations involve the pressure and the saturation of the fluid phases. For these two types of unknowns, the formulations can be derived as: "the pressure form" in which the state variables are the fluid pressures, "the saturation form" where the saturation of the fluid phases set as primary variables and "the mixed form" in which both pressure and saturation appear as unknowns [14]. Since, it is infeasible to model the saturated regions with the saturation form of flow equations, this approach is not well adopted. Also, because of the assumption of the deforming porous media, the solid skeleton displacement is set as the third independent variable. For the mixed form, Li [15] and Li et al. [16] developed a model based on state variables including degree of water saturation, pore water pressure and solid displacement for the water–oil and water–air systems, respectively. In Ref. [17], formulations based on gas pressure, water

* Corresponding author.
E-mail addresses: roza_asadi@mehr.sharif.ir (R. Asadi), ataie@sharif.edu (B. Ataie-Ashtiani).

http://dx.doi.org/10.1016/j.compgeo.2015.02.004
0266-352X/

saturation and displacement as primary variables have been proposed in a water and gas system. For the pressure form, in [6,9,18–20] the pressures of the wetting and non-wetting phase act as basic variables, while in [13,21–23] capillary pressure is one of the related primary variables. Comparative studies on selecting primary variables in the case of a rigid porous media has been discussed in the literature [14,24–28]. Numerical simulation based on pressure form, provides unique and continuous solution. Models of this type could be used in both unsaturated and saturated zones, but the method suffers from poor mass balance [14,24,26]. In contrast, mixed form achieves a better mass balance. Also, in [14] the mixed form of multiphase flow has been linearized with a modified Picard iteration which results in excellent mass balance accuracy.

In the cases where solid deformation is involved, due to the above mentioned advantages the pressure form has been extensively used. In [29] the mass conservation errors have been examined for the coupled geomechanics and multiphase flow for two problems in water–oil reservoir. Since, in modeling multiphase flow in a deformable porous media, most attention has been paid to stability and convergence properties and in comparison little effort has been directed to mass conservation analysis, in this research a detailed comparative study has been performed on this aspect alongside of the stability and convergence criteria.

Due to the highly nonlinear nature of the governing system of equations, numerical discretization should be implemented. Different spatial techniques have been used to solve the coupled equations. The finite element method is the most popular in soil consolidation problems and geotechnical engineering [6–9,11,13,18,20,22,23,30]. Despite advantages of this method in dealing with complex geometries and unstructured grids, numerical instabilities can occur for the standard finite element when strong pressure gradients appear [31–34]. The other numerical method which is widely used in the reservoir problems is finite volume method (FVM). This computational scheme preserves local conservation and is capable of capturing more accurate solution for heterogeneous material and especially at the discontinuities, as illustrated in [35]. In [31], the finite volume method has been employed for discretization of the two-phase flow and the nodal based finite element scheme for the mechanical equation. The proposed model has been verified for the water-flooding problem in an oil reservoir. Also, in [36,37], finite volume method has been used to solve the Richards equation in a rigid soil. Because of the advantages of the FVM in local conservation at the element level and eliminating pressure oscillations, this approach has been implemented in this study to solve the coupled hydro-mechanical problem.

In order to solve the hydro-mechanical coupled set of equations, two strategies can be used, first the fully coupled approach and second the sequential algorithm [35,38–40]. There are several types of sequential methods based on the different degrees of coupling which can be categorized into iteratively, explicit and loosely coupled schemes [35,38–40]. In a fully coupled fashion, one matrix system is built to solve simultaneously the equilibrium equation and the continuity equations for the immiscible flowing fluids [17,30,41–44]. Despite the stability and convergence properties of this scheme, computational cost is the issue which may make the algorithm inefficient. In contrast, by using sequential strategies, computational speed will improve, while accuracy, stability and convergence properties are affected. Among the sequential schemes, the iteratively coupled with tight convergence criteria provide higher accuracy which also has the flexibility and modularity properties of the staggered schemes [29,35,45,46]. In this approach, the coupled system of equations is split into two subproblems, which are the geomechanical equilibrium and the mass balance equations of the fluid phases. The data exchange is performed iteratively between these two portions at each time step until convergence is achieved. To overcome convergence problems which the sequential schemes deal with, different operator splits, namely, drained, undrained, fixed-strain and fixed-stress splits, have been proposed [35,46–48]. Stability analysis indicates that among these operator splits, fixed-stress split is unconditionally stable for the backward Euler time discretization, even in an incompressible system [31,46,48] and takes less number of iterations to converge [35,48]. In this method the flow equations are solved first by freezing the time-variation of the volumetric stress [31,46,48]. This method has been addressed in this paper to solve the coupled system of equations. The other sequential schemes including explicit and loosely coupled suffer from low accuracy [35] and are not included in this research.

The objectives of this study are to compare different forms of the multiphase flow in poroelastic media including pressure form, mixed form and mixed form with a modified Picard linearization in terms of stability, convergence and mass conservation, in the context of FVM. Moreover, two coupling methods of fully coupled and iteratively coupled are presented for the coupled multiphase flow and geomechanics in the presence of capillarity and the accuracy and efficiency of these two schemes are analyzed. To authors' knowledge this work is the first systematic comparative study of mathematical formulations and numerical coupling strategies for two-phase flow in deforming porous media.

Mathematical models for coupled multiphase flow and geomechanics, based on the different sets of primary variables are derived in Section 2. In Section 3, the finite volume formulations of different forms of the governing equations are generated and then, the coupling strategies are illustrated. Numerical results and comparisons are presented in Section 4, and some conclusions are drawn at the end.

2. Mathematical formulations and governing equations

The full dynamic behavior of multiphase systems based on averaging theories and a classical point of view on Biot's theory is developed in [7]. Since throughout this paper the numerical solution of the resulting governing equations is dealt with, the mathematical model using Biot's theory has been presented. In this physical approach, the mass balance equation for the solid phase can be written as [7]

$$\frac{\partial(1-n)\rho_s}{\partial t} + div((1-n)\rho_s \mathbf{v}_s) = 0 \tag{1}$$

where n is the porosity of the medium, ρ_s is the density of the solid phase, t is time and $\mathbf{v}_s$ is the solid phase velocity. Also the mass conservation equation for each fluid phase can be expressed as follows

$$\frac{\partial(nS_\alpha\rho_\alpha)}{\partial t} + div(nS_\alpha\rho_\alpha \mathbf{v}_\alpha) = 0 \tag{2}$$

where S_α, ρ_α and $\mathbf{v}_\alpha$ are the degree of saturation, density and absolute velocity of the fluid phase α, respectively. To formulate final forms of continuity equations, the time derivative of the above equations are expanded and then Eq. (1) divided by ρ_s, is added to Eq. (2) divided by $S_\alpha\rho_\alpha$. By introducing relative velocities of flowing phases with respect to the solid phase as $\mathbf{v}_{\alpha s} = \mathbf{v}_\alpha - \mathbf{v}_s$ and the material time derivative as $\frac{D(*)}{Dt} = \frac{\partial(*)}{\partial t} + div(*).\ \mathbf{v}_s$, we have [7]:

$$\frac{(1-n)}{\rho_s}\frac{D\rho_s}{Dt} + div\ \mathbf{v}_s + \frac{n}{\rho_\alpha}\frac{D\rho_\alpha}{Dt} + \frac{n}{S_\alpha}\frac{DS_\alpha}{Dt} + \frac{1}{S_\alpha\rho_\alpha} div(nS_\alpha\rho_\alpha \mathbf{v}_{\alpha s}) = 0 \tag{3}$$

By considering the solid and fluid phases as compressible, constitutive relationships for the material time derivatives of the densities of these phases are needed for the case of isothermal condition.

For the slightly compressible fluids (e.g. water and oil) this relation is as follows [7]:

$$\frac{1}{\rho_\alpha}\frac{D\rho_\alpha}{Dt}=\frac{1}{K_\alpha}\frac{Dp_\alpha}{Dt} \tag{4}$$

in which p_α and K_α are the pressure and the bulk modulus of the fluid phase α, respectively. For the gas phase, by assuming ideal gas behavior, the constitutive relationship can be written as follows [7]:

$$\frac{1}{\rho_g}\frac{D\rho_g}{Dt}=\frac{1}{p_g}\frac{Dp_g}{Dt} \tag{5}$$

As the above equation shows, for a perfect gas the bulk modulus varies directly with pressure ($K_g = p_g$). In the cases where the pressure of the gas phase (air pressure) remains close to the standard atmospheric pressure, K_g can be considered constant and equal to this datum. This assumption is valid for the cases presented in this study. Also for the solid phase, we have [7]:

$$\frac{1}{\rho_s}\frac{D\rho_s}{Dt}=\frac{1}{1-n}\left[(b-n)\frac{1}{K_s}\frac{D\bar{p}}{Dt}-(1-b)div\,\mathbf{v}_s\right] \tag{6}$$

where b is the Biot coefficient and defined as $b=1-\frac{K_T}{K_s}$, K_T and K_s are the bulk modulus of the porous medium and the solid grain respectively and $\bar{p}$ denotes the average pore pressure which for a two-phase flow system calculated from $\bar{p}=\sum_{\alpha=w,nw}p_\alpha S_\alpha$ (i.e. summation on wetting and non-wetting fluid phases). Also the term $div\,\mathbf{v}_s$ is given by [7]:

$$div\,\mathbf{v}_s=\frac{\partial\varepsilon_v}{\partial t} \tag{7}$$

where ε_v is the volumetric strain. By substituting Eqs. (4)–(7) into Eq. (3) and introducing Darcy's linear flow law for the relative velocities of the fluid phases, the resultant expressions for the continuity equations of wetting and non-wetting fluids are obtained as follows:

$$\begin{aligned}&\left(\frac{b-n}{K_s}S_w^2+\frac{nS_w}{K_w}\right)\frac{\partial p_w}{\partial t}+\left(\frac{b-n}{K_s}S_wS_{nw}\right)\frac{\partial p_{nw}}{\partial t}\\&+bS_w\frac{\partial\varepsilon_v}{\partial t}-\left(\frac{b-n}{K_s}S_wp_c-n\right)\frac{\partial S_w}{\partial t}\\&+\frac{1}{\rho_w}div\left(\rho_w\frac{\mathbf{k}k_{rw}}{\mu_w}(-grad\;p_w+\rho_w\mathbf{g})\right)=0\end{aligned} \tag{8}$$

$$\begin{aligned}&\left(\frac{b-n}{K_s}S_wS_{nw}\right)\frac{\partial p_w}{\partial t}+\left(\frac{b-n}{K_s}S_{nw}^2+\frac{nS_{nw}}{K_{nw}}\right)\frac{\partial p_{nw}}{\partial t}\\&+bS_{nw}\frac{\partial\varepsilon_v}{\partial t}-\left(\frac{b-n}{K_s}S_{nw}p_c+n\right)\frac{\partial S_w}{\partial t}\\&+\frac{1}{\rho_{nw}}div\left(\rho_{nw}\frac{\mathbf{k}k_{rnw}}{\mu_{nw}}(-grad\;p_{nw}+\rho_{nw}\mathbf{g})\right)=0\end{aligned} \tag{9}$$

where $\mathbf{k}$ is the intrinsic permeability tensor, k_w and k_{nw} are the relative permeabilities of the wetting and non-wetting phases which are functions of degree of saturation. μ_w and μ_{nw} denote the dynamic viscosities of the two fluid phases, $\mathbf{g}$ is the gravity vector and p_c is the capillary pressure which is defined as $p_c = p_{nw} - p_w$ and also can be determined experimentally as a function of degree of saturation. Here, the intrinsic permeability is considered to remain constant, which is a general assumption in standard reservoir simulations and the problems deal with modeling the partially saturated soils. In addition, hysteresis effects are ignored.

Under the quasi-static condition, the linear momentum balance equation for the multiphase medium can be expressed as follows [7]

$$div\,\boldsymbol{\sigma}+\rho_b\mathbf{f}=0 \tag{10}$$

in which $\boldsymbol{\sigma}$ is the total stress tensor, $\mathbf{f}$ is the body force and ρ_b is the bulk density which is defined as $\rho_b=(1-n)\rho_s+n(S_w\rho_w+S_{nw}\rho_{nw})$. The equation which relates the total stress to the pore pressure of the fluid phases and the effective stress, for the compressible solid grains can be written as [7]:

$$\boldsymbol{\sigma}=\boldsymbol{\sigma}''-b\mathbf{I}\bar{p} \tag{11}$$

In which $\boldsymbol{\sigma}''$ is the modified effective stress tensor which causes the deformations of the solid skeleton and $\mathbf{I}$ is the second-order unit tensor. By assuming linear elastic behavior, the modified effective stress can be defined as a function of total strain, as follows

$$\frac{\partial\boldsymbol{\sigma}''}{\partial t}=\boldsymbol{D}\frac{\partial\boldsymbol{\varepsilon}}{\partial t} \tag{12}$$

where $\boldsymbol{D}$ represents the elastic stiffness tensor and $\boldsymbol{\varepsilon}$ is the total strain tensor.

Introducing definitions (11) and (12) into Eq. (10) and differentiating the resulting equation with respect to time [6,30,9,18], yields to the following equation of geomechanical equilibrium.

$$div\left(\boldsymbol{D}\frac{\partial\boldsymbol{\varepsilon}}{\partial t}-b\mathbf{I}\frac{\partial\bar{p}}{\partial t}\right)=\rho_b\frac{\partial\mathbf{f}}{\partial t} \tag{13}$$

2.1. Primary variable selection

To derive a fully coupled system to simultaneously solve the mass balance and the mechanical equilibrium equations, appropriate choice of primary variables is essential and reformulation of Eqs. (8), (9) and (13) in terms of these selected variables are required. For this purpose two types of primary variables are selected. In the first type, formulations are based on the pressure of fluid phases and in the second type, saturation and the pressure of the wetting phase are the unknown variables. The mathematical equations are developed in the following sections and appropriate constitutive relationships are implemented in each case.

2.1.1. Pressure form

In this form of formulations, the displacement and the pressure of fluid phases are selected as a set of state variables. Based on the capillary pressure–saturation relationship and by applying the chain rule, the term $\frac{\partial S_w}{\partial t}$ can be rewritten in the following way [9]

$$\frac{\partial S_w}{\partial t}=\frac{dS_w}{dp_c}\frac{\partial p_c}{\partial t}=\frac{dS_w}{dp_c}\left(\frac{\partial p_{nw}}{\partial t}-\frac{\partial p_w}{\partial t}\right) \tag{14}$$

The sum of saturations of all fluid phases is equal to unity, so by imposing the constraint $\sum_{\alpha=w,nw}S_\alpha=1$ and substituting expression (14) into Eqs. (8) and (9), the pressure form of mass flow equations are derived as follows:

$$\begin{aligned}&\left[\frac{b-n}{K_s}S_w^2+\frac{nS_w}{K_w}+\left(\frac{b-n}{K_s}S_wp_c-n\right)\frac{dS_w}{dp_c}\right]\frac{\partial p_w}{\partial t}\\&+\left[\frac{b-n}{K_s}S_w(1-S_w)-\left(\frac{b-n}{K_s}S_wp_c-n\right)\frac{dS_w}{dp_c}\right]\frac{\partial p_{nw}}{\partial t}+bS_w\frac{\partial\varepsilon_v}{\partial t}\\&+\frac{1}{\rho_w}div\left[\rho_w\frac{\mathbf{k}k_{rw}}{\mu_w}(-grad\;p_w+\rho_w\mathbf{g})\right]=0\end{aligned} \tag{15}$$

$$\begin{aligned}&\left[\frac{b-n}{K_s}S_w(1-S_w)+\left(\frac{b-n}{K_s}(1-S_w)p_c+n\right)\frac{dS_w}{dp_c}\right]\frac{\partial p_w}{\partial t}\\&+\left[\frac{b-n}{K_s}(1-S_w)^2+\frac{n(1-S_w)}{K_{nw}}-\left(\frac{b-n}{K_s}(1-S_w)p_c+n\right)\frac{dS_w}{dp_c}\right]\frac{\partial p_{nw}}{\partial t}\\&+b(1-S_w)\frac{\partial\varepsilon_v}{\partial t}+\frac{1}{\rho_{nw}}div\left[\rho_{nw}\frac{\mathbf{k}k_{rnw}}{\mu_{nw}}(-grad\;p_{nw}+\rho_{nw}\mathbf{g})\right]=0\end{aligned} \tag{16}$$

In the same manner, the rate of the average pore pressure in the geomechanical equation can be determined as [9]:

$$\frac{\partial \bar{p}}{\partial t} = S_w \frac{\partial p_w}{\partial t} + S_{nw} \frac{\partial p_{nw}}{\partial t} + p_w \frac{\partial S_w}{\partial t} + p_{nw} \frac{\partial S_{nw}}{\partial t} = \left(S_w + p_c \frac{dS_w}{dp_c}\right) \frac{\partial p_w}{\partial t} + \left(1 - S_w - p_c \frac{dS_w}{dp_c}\right) \frac{\partial p_{nw}}{\partial t} \tag{17}$$

Finally, applying Eq. (17) into Eq. (13), leads to the following expression for the pressure form of the geomechanical equation:

$$div \left[\boldsymbol{D} \frac{\partial \boldsymbol{\varepsilon}}{\partial t} - b\mathbf{I}\left(\left(S_w + p_c \frac{dS_w}{dp_c}\right) \frac{\partial p_w}{\partial t} + \left(1 - S_w - p_c \frac{dS_w}{dp_c}\right) \frac{\partial p_{nw}}{\partial t}\right)\right] = \rho_b \frac{\partial \mathbf{f}}{\partial t} \tag{18}$$

2.1.2. Mixed form

In the mixed form, the displacement of the solid skeleton, pore water pressure and the degree of water saturation are taken as the independent variables. Since capillary pressure is considered as a function of saturation, i.e. $p_c = f(S_w)$, by imposing this constraint the mass conservation equations can be written as follows

$$\left[\left(\frac{b-n}{K_s} + \frac{n}{K_w}\right) S_w\right] \frac{\partial p_w}{\partial t} + \left[\left(\frac{b-n}{K_s} S_w (1 - S_w)\right) \frac{dp_c}{dS_w} - \left(\frac{b-n}{K_s} S_w\right) p_c + n\right] \frac{\partial S_w}{\partial t} + bS_w \frac{\partial \varepsilon_v}{\partial t} + \frac{1}{\rho_w} div \left[\rho_w \frac{\mathbf{k} k_{rw}}{\mu_w} (-grad\ p_w + \rho_w \mathbf{g})\right] = 0 \tag{19}$$

$$\left[\left(\frac{b-n}{K_s} + \frac{n}{K_{nw}}\right)(1 - S_w)\right] \frac{\partial p_w}{\partial t} + \left[\left(\frac{b-n}{K_s}(1 - S_w)^2 + \frac{n(1 - S_w)}{K_{nw}}\right) \frac{dp_c}{dS_w} - \left(\frac{b-n}{K_s}(1 - S_w)\right) p_c - n\right] \frac{\partial S_w}{\partial t} + bS_{nw} \frac{\partial \varepsilon_v}{\partial t} + \frac{1}{\rho_{nw}} div \left[\rho_{nw} \frac{\mathbf{k} k_{rnw}}{\mu_{nw}} (-grad\ (p_w + p_c) + \rho_{nw} \mathbf{g})\right] = 0 \tag{20}$$

Also, with respect to the primary variables (i.e., pressure, saturation and displacement), the geomechanical equation takes the following form

$$div \left[\boldsymbol{D} \frac{\partial \boldsymbol{\varepsilon}}{\partial t} - b\mathbf{I}\left(\frac{\partial p_w}{\partial t} + \left((1 - S_w) \frac{dp_c}{dS_w} - p_c\right) \frac{\partial S_w}{\partial t}\right)\right] = \rho_b \frac{\partial \mathbf{f}}{\partial t} \tag{21}$$

2.2. Initial and boundary conditions

The above equations form a coupled hydro-mechanical system defined on a domain Ω bounded by the boundary Γ. To complete the mathematical formulations, the initial and boundary conditions associated with each type of primary unknowns can be expressed as follows:

2.2.1. Primary variables: $p_w, p_{nw}, \mathbf{u}$

For this set of primary variables, the initial and boundary conditions could be defined as follows:

– Initial conditions

$$\begin{cases} \mathbf{u} = \mathbf{u}^0 \\ p_\alpha = p_\alpha^0 \end{cases} \quad \alpha = w, nw \quad \text{at } t = 0 \text{ and on } \Omega \tag{22}$$

$\mathbf{u}^0$ and p_α^0, are the initial value of the displacement and the α-phase pressure, respectively.

– Boundary conditions

$$\begin{cases} \mathbf{u} = \mathbf{u_D} & \text{on } \Gamma_u \\ \sigma'' \cdot \mathbf{n} = \mathbf{S_D} & \text{on } \Gamma_t \\ p_\alpha = p_{\alpha_D} & \text{on } \Gamma_p \\ \frac{\mathbf{k} k_\alpha}{\mu_\alpha} (-grad\ (p_\alpha) + \rho_\alpha \mathbf{g}) \cdot \mathbf{n} = \mathbf{q}_\alpha & \text{on } \Gamma_q \end{cases} \tag{23}$$

$\mathbf{u_D}$ and $\mathbf{S_D}$ are the prescribed displacement and traction, respectively on the corresponding boundaries, namely Γ_u and Γ_t, whereas p_{α_D} and $\mathbf{q}_\alpha$ denote the imposed pore pressure and flux of fluid phase α, on the boundaries Γ_p and Γ_q, respectively and $\mathbf{n}$ is the unit normal vector of the boundary [9]. Γ_u and Γ_p correspond to the Dirichet boundary condition for the displacement and the α-phase pressure, respectively. Also Γ_t and Γ_q are the Neumann type boundary conditions. In Eqs. (22) and (23), $\Gamma_u \cup \Gamma_t = \Gamma_p \cup \Gamma_q = \Gamma$ and $\Gamma_u \cap \Gamma_t = \Gamma_p \cap \Gamma_q = \emptyset$.

2.2.2. Primary variables: p_w, S_w, u

For this type of primary variables, we have:

– Initial conditions

$$\begin{cases} \mathbf{u} = \mathbf{u^0} \\ p_w = p_w^0 \\ S_w = S_w^0 \end{cases} \quad \text{at } t = 0 \text{ and on } \Omega \tag{24}$$

p_w^0 and S_w^0 denote the initial value of water pressure and water saturation, respectively.

– Boundary conditions

For the Neumann boundary conditions the equations are the same, while for the Dirichlet boundary condition, we have

$$\begin{cases} \mathbf{u} = \mathbf{u_D} & \text{on } \Gamma_u \\ p_w = p_{w_D} \text{ and } S_w = S_{w_D} & \text{on } \Gamma_p \end{cases} \tag{25}$$

where p_{w_D} and S_{w_D} are the prescribed value of water pressure and saturation on the boundary Γ_p, respectively.

3. Numerical model

Following the general procedure of the FVM, first the solution domain is subdivided into a number of finite volumes in such a way that a dual mesh of control volumes is generated. In this staggered grid arrangement, two different spatial grids are used: one for the discretization of the pressure and saturation unknowns and the other for the displacements. In a one-dimensional simulation, the control volumes and the location of the solution variables are depicted in Fig. 1. This space discretization strategy preserves mass conservation at the element level, yields continuous displacement field and leads to higher accuracy for stresses and fluxes at the interfaces [35,46,49,50]. Also for temporal discretization, a grid in time with a step-size Δt is employed. According to these grids, the notations for discrete parameters are introduced as follows

$$\begin{aligned} u &:= u^n := u_i^n := u(z_{i-0.5}, t_n), \\ p_\alpha &:= p_\alpha^n := p_{\alpha_i}^n := p_\alpha(z_i, t_n), \\ S_\alpha &:= S_\alpha^n := S_{\alpha_i}^n := S_\alpha(z_i, t_n), \quad \alpha = w, nw \end{aligned} \tag{26}$$

where p_α^n, S_α^n and u^n are the α-phase pressure, saturation and displacement at time t_n. $p_{\alpha_i}^n$ and $S_{\alpha_i}^n$ denote α-phase pressure and saturation at node i and u_i^n refers to displacement at node $i - 0.5$.

In the next step, by integrating the flow equations on a control volume $(z_{i-0.5}, z_{i+0.5})$ and the mechanical equation on (z_{i-1}, z_i), the

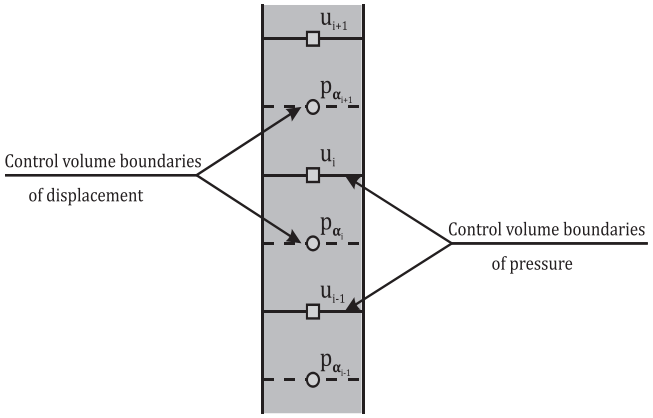

Fig. 1. Staggered grid and control volumes in one dimension.

finite volume scheme is obtained. The detailed formulations for each form of equations are described in the following sections. Also for discretization of the time derivative, as included by many authors, unconditional stability would be obtained for a time weighting factor greater than 0.5 [9,13,51]. Therefore, as considered in [30,13,19] fully implicit time discretization has been performed in this research.

In order to solve the resulting non-linear coupled system of equations, iterative schemes are required to deal with nonlinearities. For linearization of the pressure and mixed form of the governing equations at each time step, the Picard iteration scheme (fixed point) has been employed because of its robustness [21]. The other procedure which can be applied to the mixed form is a modified Picard linearization. Within this approach the pressure of the fluid phases and the displacement are used as the primary variables for the solution at a new iteration step. To solve nonlinear forms of multiphase equations during the iteration process, different convergence criterions have been suggested and utilized for the rigid [28,52,53] and deformable porous media [6,9,54]. In this study convergence criterions which are based on a maximum difference of the state variables between successive time steps have been used as

$$\begin{aligned}
&\max\left|\frac{p_\alpha^{n+1,k+1}-p_\alpha^{n+1,k}}{p_\alpha^{n+1,k+1}}\right|\leqslant\epsilon_p\\
&\max\left|\frac{S_w^{n+1,k+1}-S_w^{n+1,k}}{S_w^{n+1,k+1}}\right|\leqslant\epsilon_s\\
&\max\left|\frac{u^{n+1,k+1}-u^{n+1,k}}{u^{n+1,k+1}}\right|\leqslant\epsilon_u
\end{aligned}\tag{27}$$

in the above equation, superscript n denotes time level and k is the iteration counter. ϵ_p, ϵ_s and ϵ_u indicate the convergence tolerance for pressure of the α-phase, saturation and displacement, respectively. The values of the convergence tolerances depend upon the desired accuracy and the physics of the problem, and are determined in each case to accelerate the convergence.

3.1. Finite volume framework

The discretized forms of the solution strategies for the uniform structured grid in one dimension (Fig. 1) are derived in the finite volume framework in the following sections.

3.1.1. Pressure form

As mentioned above, by employing FVM for discretization of the differential problems (15) and (16) over a control volume $(z_{i-0.5}, z_{i+0.5})$ and introducing the volumetric strain for a one-dimensional simulation as $\varepsilon_v=\frac{\partial u}{\partial z}$, full discretizations for the pressure form of the wetting and non-wetting phases, respectively, yield:

$$\begin{aligned}
&\left[\frac{b-n}{K_s}\left(S_{w_i}^{n+1,k}\right)^2+\frac{nS_{w_i}^{n+1,k}}{K_w}+\left(\frac{b-n}{K_s}S_{w_i}^{n+1,k}p_{c_i}^{n+1,k}-n\right)\left(\frac{dS_w}{dp_c}\right)_i^{n+1,k}\right]\\
&\times\left(\frac{p_{w_i}^{n+1,k+1}-p_{w_i}^n}{\Delta t}\right)+\left[\frac{b-n}{K_s}S_{w_i}^{n+1,k}\left(1-S_{w_i}^{n+1,k}\right)\right.\\
&\left.-\left(\frac{b-n}{K_s}S_{w_i}^{n+1,k}p_{c_i}^{n+1,k}-n\right)\left(\frac{dS_w}{dp_c}\right)_i^{n+1,k}\right]\\
&\times\left(\frac{p_{nw_i}^{n+1,k+1}-p_{nw_i}^n}{\Delta t}\right)+\frac{bS_{w_i}^{n+1,k}}{\Delta z}\left(\frac{u_{i+1}^{n+1,k+1}-u_{i+1}^n}{\Delta t}-\frac{u_i^{n+1,k+1}-u_i^n}{\Delta t}\right)\\
&+\left[-\kappa_{w_{i+1}}^{n+1,k}\left(\frac{p_{w_{i+1}}^{n+1,k+1}-p_{w_i}^{n+1,k+1}}{\Delta z^2}\right)+\kappa_{w_i}^{n+1,k}\left(\frac{p_{w_i}^{n+1,k+1}-p_{w_{i-1}}^{n+1,k+1}}{\Delta z^2}\right)\right.\\
&\left.+\gamma_w\left(\frac{\kappa_{w_{i+1}}^{n+1,k}-\kappa_{w_i}^{n+1,k}}{\Delta z}\right)\right]=0
\end{aligned}\tag{28}$$

$$\begin{aligned}
&\left[\frac{b-n}{K_s}S_{w_i}^{n+1,k}\left(1-S_{w_i}^{n+1,k}\right)+\left(\frac{b-n}{K_s}\left(1-S_{w_i}^{n+1,k}\right)p_{c_i}^{n+1,k}+n\right)\left(\frac{dS_w}{dp_c}\right)_i^{n+1,k}\right]\\
&\times\left(\frac{p_{w_i}^{n+1,k+1}-p_{w_i}^n}{\Delta t}\right)+\left[\frac{b-n}{K_s}\left(1-S_{w_i}^{n+1,k}\right)^2+\frac{n(1-S_{w_i}^{n+1,k})}{K_{nw}}\right.\\
&\left.-\left(\frac{b-n}{K_s}(1-S_{w_i}^{n+1,k})p_{c_i}^{n+1,k}+n\right)\left(\frac{dS_w}{dp_c}\right)_i^{n+1,k}\right]\left(\frac{p_{nw_i}^{n+1,k+1}-p_{nw_i}^n}{\Delta t}\right)\\
&+\frac{b(1-S_{w_i}^{n+1,k})}{\Delta z}\left(\frac{u_{i+1}^{n+1,k+1}-u_{i+1}^n}{\Delta t}-\frac{u_i^{n+1,k+1}-u_i^n}{\Delta t}\right)\\
&+\left[-\kappa_{nw_{i+1}}^{n+1,k}\left(\frac{p_{nw_{i+1}}^{n+1,k+1}-p_{nw_i}^{n+1,k+1}}{\Delta z^2}\right)+\kappa_{nw_i}^{n+1,k}\left(\frac{p_{nw_i}^{n+1,k+1}-p_{nw_{i-1}}^{n+1,k+1}}{\Delta z^2}\right)\right.\\
&\left.+\gamma_{nw}\left(\frac{\kappa_{nw_{i+1}}^{n+1,k}-\kappa_{nw_i}^{n+1,k}}{\Delta z}\right)\right]=0
\end{aligned}\tag{29}$$

κ_w and κ_{nw} are the interblock hydraulic conductivity of the wetting and non-wetting phases, respectively and evaluated as the arithmetic mean as follows

$$\begin{aligned}
\kappa_\alpha &:= \kappa_\alpha^n := \kappa_{\alpha_i}^n := \kappa_\alpha(z_{i-0.5},t_n)\\
&=\frac{\frac{\mathbf{k}k_{r\alpha}}{\mu_\alpha}(z_i,t_n)+\frac{\mathbf{k}k_{r\alpha}}{\mu_\alpha}(z_{i-1},t_n)}{2}\quad\alpha=w,nw
\end{aligned}\tag{30}$$

To discretize the mechanical equation, the stress–strain relationship for a linear elastic porous medium is implemented in Eq. (18) and the resulting equation is integrated over each interval (z_{i-1}, z_i), which leads to:

$$\begin{aligned}
&\frac{K_{dr_i}}{\Delta z}\left(\frac{u_{i+1}^{n+1,k+1}-u_{i+1}^n}{\Delta t}-\frac{u_i^{n+1,k+1}-u_i^n}{\Delta t}\right)\\
&-\frac{K_{dr_{i-1}}}{\Delta z}\left(\frac{u_i^{n+1,k+1}-u_i^n}{\Delta t}-\frac{u_{i-1}^{n+1,k+1}-u_{i-1}^n}{\Delta t}\right)\\
&-b\left(S_{w_i}^{n+1,k}+p_{c_i}^{n+1,k}\left(\frac{dS_w}{dp_c}\right)_i^{n+1,k}\right)\left(\frac{p_{w_i}^{n+1,k+1}-p_{w_i}^n}{\Delta t}\right)\\
&+b\left(S_{w_{i-1}}^{n+1,k}+p_{c_{i-1}}^{n+1,k}\left(\frac{dS_w}{dp_c}\right)_{i-1}^{n+1,k}\right)\left(\frac{p_{w_{i-1}}^{n+1,k+1}-p_{w_{i-1}}^n}{\Delta t}\right)\\
&-b\left(1-S_{w_i}^{n+1,k}-p_{c_i}^{n+1,k}\left(\frac{dS_w}{dp_c}\right)_i^{n+1,k}\right)\left(\frac{p_{nw_i}^{n+1,k+1}-p_{nw_i}^n}{\Delta t}\right)\\
&+b\left(1-S_{w_{i-1}}^{n+1,k}-p_{c_{i-1}}^{n+1,k}\left(\frac{dS_w}{dp_c}\right)_{i-1}^{n+1,k}\right)\left(\frac{p_{nw_{i-1}}^{n+1,k+1}-p_{nw_{i-1}}^n}{\Delta t}\right)\\
&=\rho_b\frac{f_i^{n+1,k}-f_i^n}{\Delta t}
\end{aligned}\tag{31}$$

where K_{dr} represents the drained bulk modulus of porous media which can be defined in terms of Young's modulus and Poisson's ratio in one dimension as $\frac{E(1-\upsilon)}{(1+\upsilon)(1-2\upsilon)}$.

3.1.2. Mixed form

In a similar manner, a mixed finite volume formulation for the coupled partial differential Eqs. (19)–(21), can be expressed as follows

$$\begin{aligned}
&\left[\left(\frac{b-n}{K_s}+\frac{n}{K_w}\right)S_{w_i}^{n+1,k}\right]\left(\frac{p_{w_i}^{n+1,k+1}-p_{w_i}^{n}}{\Delta t}\right)\\
&+\left[\left(\frac{b-n}{K_s}S_{w_i}^{n+1,k}\left(1-S_{w_i}^{n+1,k}\right)\right)\left(\frac{dp_c}{dS_w}\right)_i^{n+1,k}-\left(\frac{b-n}{K_s}S_{w_i}^{n+1,k}\right)p_{c_i}^{n+1,k}+n\right]\\
&\times\left(\frac{S_{w_i}^{n+1,k+1}-S_{w_i}^{n}}{\Delta t}\right)+\frac{bS_{w_i}^{n+1,k}}{\Delta z}\left(\frac{u_{i+1}^{n+1,k+1}-u_{i+1}^{n}}{\Delta t}-\frac{u_{i}^{n+1,k+1}-u_{i}^{n}}{\Delta t}\right)\\
&+\left[-\kappa_{w_{i+1}}^{n+1,k}\left(\frac{p_{w_{i+1}}^{n+1,k+1}-p_{w_i}^{n+1,k+1}}{\Delta z^2}\right)+\kappa_{w_i}^{n+1,k}\left(\frac{p_{w_i}^{n+1,k+1}-p_{w_{i-1}}^{n+1,k+1}}{\Delta z^2}\right)\right.\\
&\left.+\gamma_w\left(\frac{\kappa_{w_{i+1}}^{n+1,k}-\kappa_{w_i}^{n+1,k}}{\Delta z}\right)\right]=0
\end{aligned}\tag{32}$$

$$\begin{aligned}
&\left[\left(\frac{b-n}{K_s}+\frac{n}{K_{nw}}\right)\left(1-S_{w_i}^{n+1,k}\right)\right]\left(\frac{p_{w_i}^{n+1,k+1}-p_{w_i}^{n}}{\Delta t}\right)\\
&+\left[\left(\frac{b-n}{K_s}(1-S_{w_i}^{n+1,k})^2+\frac{n(1-S_{w_i}^{n+1,k})}{K_{nw}}\right)\left(\frac{dp_c}{dS_w}\right)_i^{n+1,k}\right.\\
&\left.-\left(\frac{b-n}{K_s}\left(1-S_{w_i}^{n+1,k}\right)\right)p_{c_i}^{n+1,k}-n\right]\left(\frac{S_{w_i}^{n+1,k+1}-S_{w_i}^{n}}{\Delta t}\right)\\
&+\frac{b\left(1-S_{w_i}^{n+1,k}\right)}{\Delta z}\left(\frac{u_{i+1}^{n+1,k+1}-u_{i+1}^{n}}{\Delta t}-\frac{u_{i}^{n+1,k+1}-u_{i}^{n}}{\Delta t}\right)\\
&+\left[-\kappa_{nw_{i+1}}^{n+1,k}\left(\frac{p_{w_{i+1}}^{n+1,k+1}+p_{c_{i+1}}^{n+1,k}-p_{w_i}^{n+1,k+1}-p_{c_i}^{n+1,k}}{\Delta z^2}\right)\right.\\
&\left.+\kappa_{nw_i^{n+1,k}}\left(\frac{p_{w_i}^{n+1,k+1}+p_{c_i}^{n+1,k}-p_{w_{i-1}}^{n+1,k+1}-p_{c_{i-1}}^{n+1,k}}{\Delta z^2}\right)\right.\\
&\left.+\gamma_{nw}\left(\frac{\kappa_{nw_{i+1}}^{n+1,k}-\kappa_{nw_i}^{n+1,k}}{\Delta z}\right)\right]=0
\end{aligned}\tag{33}$$

$$\begin{aligned}
&\frac{K_{dr_i}}{z}\left(\frac{u_{i+1}^{n+1,k+1}-u_{i+1}^{n}}{\Delta t}-\frac{u_{i}^{n+1,k+1}-u_{i}^{n}}{\Delta t}\right)\\
&-\frac{K_{dr_{i-1}}}{z}\left(\frac{u_{i}^{n+1,k+1}-u_{i}^{n}}{\Delta t}-\frac{u_{i-1}^{n+1,k+1}-u_{i-1}^{n}}{\Delta t}\right)\\
&-b\left(\frac{p_{w_i}^{n+1,k+1}-p_{w_i}^{n}}{\Delta t}\right)+b\left(\frac{p_{w_{i-1}}^{n+1,k+1}-p_{w_{i-1}}^{n}}{\Delta t}\right)\\
&-b\left(\left(1-S_{w_i}^{n+1,k}\right)\left(\frac{dp_c}{dS_w}\right)_i^{n+1,k}-p_{c_i}^{n+1,k}\right)\left(\frac{S_{w_i}^{n+1,k+1}-S_{w_i}^{n}}{\Delta t}\right)\\
&+b\left(\left(1-S_{w_{i-1}}^{n+1,k}\right)\left(\frac{dp_c}{dS_w}\right)_{i-1}^{n+1,k}-p_{c_{i-1}}^{n+1,k}\right)\left(\frac{S_{w_{i-1}}^{n+1,k+1}-S_{w_{i-1}}^{n}}{\Delta t}\right)\\
&=\rho_b\frac{f_i^{n+1,k}-f_i^{n}}{\Delta t}
\end{aligned}\tag{34}$$

For the above equation, the discretized form of the term $\left((1-S_w)\frac{dp_c}{dS_w}\right)\frac{\partial S_w}{\partial t}$ in Eq. (21) can also be written as $\left(1-S_{w_i}^{n+1,k}\right)\left(\frac{p_{c_i}^{n+1,k}-p_{c_i}^{n}}{\Delta t}\right)$.

3.1.3. Mixed form with a modified Picard linearization

In this approach, the time derivative of saturation is approximated using a first-order Taylor expansion and by incorporating with the Picard iteration, can be written in discrete terms as [14]:

$$\frac{S_\alpha^{n+1,k+1}-S_\alpha^{n}}{\Delta t}\approx\frac{S_\alpha^{n+1,k}+\left(\frac{dS_\alpha}{dp_c}\right)^{n+1,k}\left(p_c^{n+1,k+1}-p_c^{n+1,k}\right)-S_\alpha^{n}}{\Delta t}\qquad \alpha=w,nw\tag{35}$$

By substituting Eq. (34) into Eqs. (31)–(33), the modified Picard approximations can be provided.

Finally, the system of algebraic equations can be written in the following matrix form:

$$\mathbf{A}\frac{d\mathbf{X}}{dt}+\mathbf{B}\mathbf{X}=\mathbf{F}\tag{36}$$

where $\mathbf{X}=[p_w,p_{nw},u]$ in the pressure and modified Picard schemes and equal to $[p_w,S_w,u]$ in the mixed form. A detailed explanation of the coefficients in the matrices **A**, **B** and **F** could be derived from the above equations.

3.2. Coupling schemes

The coupled system of equations presented above can be solved with two numerical solution algorithms: fully coupled approach and the sequential method. For the sequential coupling strategies, fixed-stress scheme has been developed in this section. In this approach, the rate of the volumetric stress ($\dot{\sigma}_v$) is kept constant during the solution of the flow equations. By implementing Picard iteration to linearize the flow equations, we have [55]:

$$\varepsilon_v^{n+1,k+1}=\varepsilon_v^{n+1,k}+\frac{b}{K_{dr}}\left(\bar{p}^{n+1,k+1}-\bar{p}^{n+1,k}\right)\tag{37}$$

By introducing the above definition for the volumetric strain at the $(k+1)$ th iteration, the term $\frac{\partial\varepsilon_v}{\partial t}$, in the flow equations can be written as:

$$\frac{\partial\varepsilon_v}{\partial t}=\frac{\varepsilon_v^{n+1,k}+\frac{b}{K_{dr}}\left(\bar{p}^{n+1,k+1}-\bar{p}^{n+1,k}\right)-\varepsilon_v^{n}}{\Delta t}\tag{38}$$

in the above equation, the term $\bar{p}$ should be substituted based on the selected primary variables. By solving the flow equations, the values for the fluid pressures and saturation are updated and then the displacements are being calculated from the mechanical equation. The flowchart of the fixed-stress split as an iteratively coupled scheme is shown in Fig. 2.

3.3. Mass balance calculations

One essential criterion to evaluate the numerical model is the global mass balance error which shows the difference between the total addition mass in the domain and the total net flux into the domain [24]. A cumulative mass balance error can be defined as follows [27]:

$$\text{cumulative error (t)}=\left|1-\frac{M_\alpha^t-M_\alpha^0}{\sum_{\Delta t}q_\alpha^{\Delta t}}\right|\tag{39}$$

where M_α^t and M_α^0 are the α- fluid mass storage at time t and at initial, respectively. $q_\alpha^{\Delta t}$ is the total net flux of the α- phase into the domain during the time step. Wan calculated the global mass balance error for two cases of primary depletion and water flooding in deformable porous media to show good properties of global mass conservation of the proposed model [29].

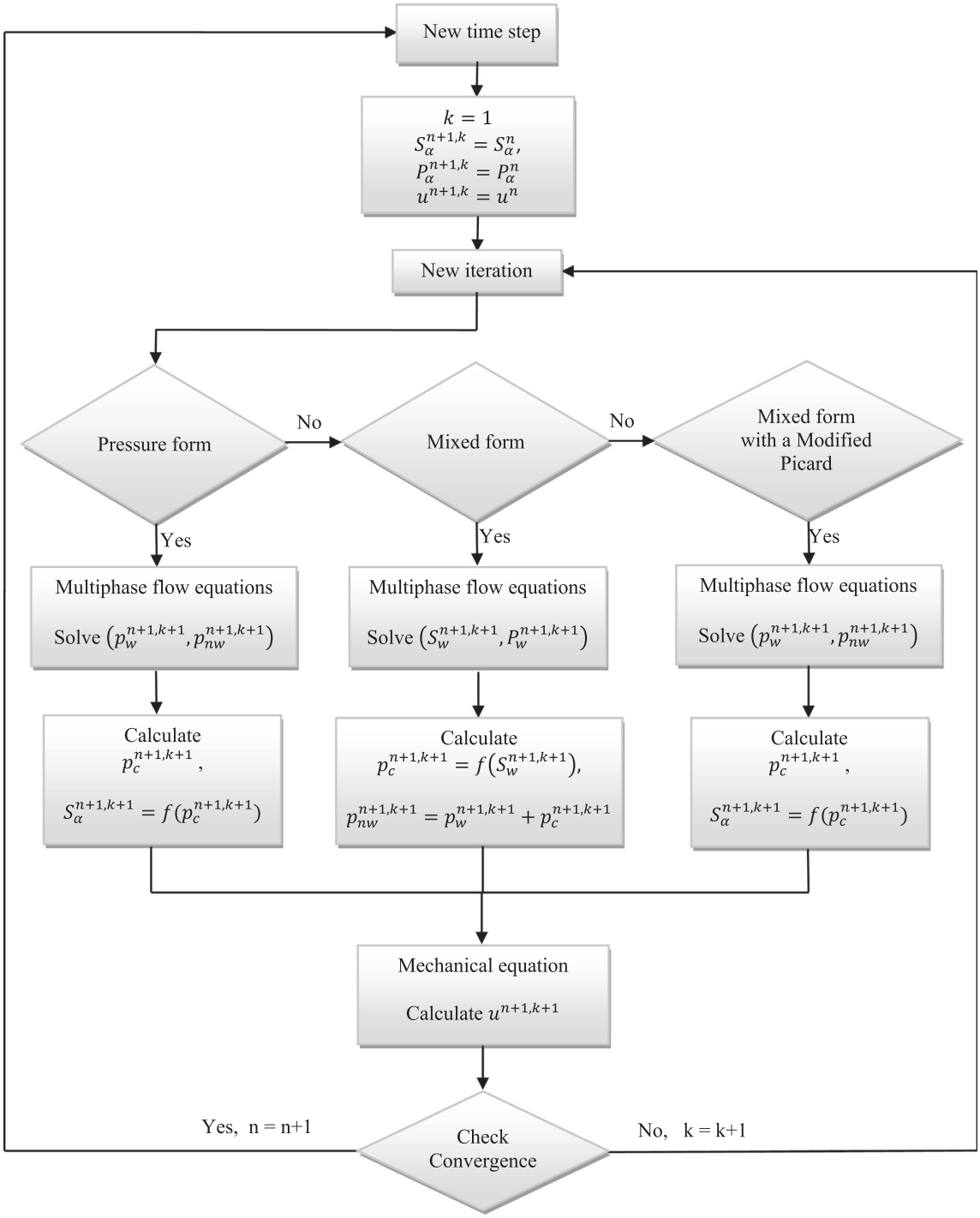

Fig. 2. Flowchart of the fixed-stress splits for the different forms of the governing equations.

4. Numerical results

The validity of the proposed models is examined through several examples, which cover most of the features in modeling the coupled two-phase flow in a poroelastic porous media. These features include; capillarity and gravity effects, compressibility of the fluid phases, water–oil and water–gas systems, the conditions near the residual saturation and the fully saturated and different boundary conditions for both the flow equations and the mechanics.

The first and second examples are the benchmark problems and show the potential of the model in the case of unsaturated deforming porous media [6,7,51]. The third and fourth problems involve an incompressible water/oil system, initially saturated with the non-wetting and wetting fluid phases, respectively [27,59,60]. In the first part, numerical modeling of different forms of the governing equations are studied and the advantages and disadvantages of each model have been discussed. In the second part different coupling schemes including fully coupled and iteratively coupled (fixed-stress) are analyzes to assess their CPU time, total iterations and the value of RMSE (root mean square errors) for pressures, saturation and displacement relative to the fully coupled approach. In this study, all of the numerical codes have been developed in

MATLAB 6.0 software and have been simulated using a serial code on an Intel® Core™ i5 CPU M540@ 2.53 GHz processor with 6 GB RAM.

4.1. Model verification and a comparison of numerical algorithms

In this section, the first and second examples have been tested by comparison against solutions which reported in the references and for the Mcwhorter problems [59], comparisons are made with the result of the analytical solutions in the rigid porous media.

4.1.1. Liakopoulos experiment: Sand column drainage

The first example is based on an experiment performed by Liakopoulos [56] which involves desaturation of a soil column due to gravitational effect. This test case has been used as a benchmark in the literature for validation of multiphase fluid flow in a deformable porous media [9,19,20,22,23]. In this experiment, a vertical soil column with a height of 1 m, consisting of Del Monte sand, is instrumented to measure moisture pressure during transient water flow. Before the start of the drainage process, a fully saturated initial condition was imposed by establishing uniform flow through a soil profile. In order to achieve this condition in the laboratory, constant water inflow and free drainage condition are applied at the top and bottom surfaces, respectively. When the measurements show zero pore pressure within the specimen, water inflow is stopped and drainage takes place from the base of the soil column under gravity. Hence, pore water pressure at the bottom is put equal to zero (i.e. the atmospheric pressure). Also, during the experiment both ends of the specimen are exposed to the atmospheric pressure, so there would be zero air pressure at the upper and lower boundaries. For the displacement field, traction-free boundary condition is applied on the top surface and vertical displacement is constrained at the bottom. The side walls are rigid and impermeable so the example can be solved as a one dimensional problem. Configuration of the problem with assumed boundary conditions before and at the beginning of the experiment is shown in Fig. 3. The initial condition prior to the start of the experiment has been illustrated in Fig. 3a. At this stage the water pressure throughout the column is equal to zero. Also in Fig. 3b the boundary condition at the initial and during the simulation is shown. In this figure, interruption of inflow at the top of the specimen has been represented with the impervious boundary condition.

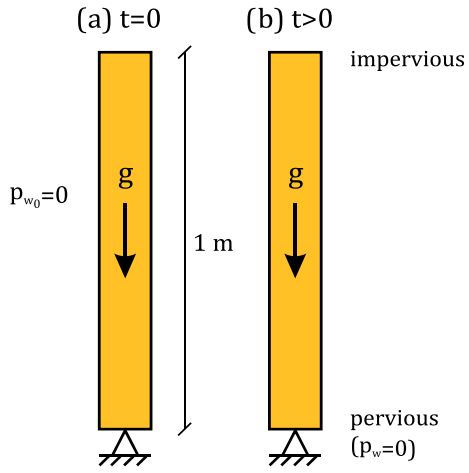

Fig. 3. Liakopoulos experiment: configuration of the problem with assumed boundary conditions (a and b).

The constitutive relationships for the water degree of saturation and the water relative permeability, which were experimentally determined by Liakopoulos, are shown in the following equations:

$$S_w = 1 - 1.9722 \times 10^{-11} p_c^{2.4279} \tag{40}$$

$$k_{rw} = 1 - 2.207(1 - S_w)^{1.0121} \tag{41}$$

Also for this two-phase flow simulation, dependency of gas relative permeability on water saturation is described by Brooks–Corey model [57]

$$k_{rg} = (1 - S_e)^2 \left(1 - S_e^{\frac{(2+\lambda)}{\lambda}}\right) \tag{42}$$

$$S_e = \frac{S_w - S_{rw}}{1 - S_{rw}} \tag{43}$$

where S_e is the effective saturation, S_{rw} is the residual water saturation and λ is the pore size distribution index. In addition, to solve the problem in fully saturated condition, the gas relative permeability is limited to a minimum value of 0.0001 [7,51]. This assumption implies that both water and airflow exist and the air phase continuity equation is always maintained [7]. Eqs. (40)–(42) have been illustrated in Figs. 4–6, respectively. Parameters of the hydraulic functions and properties of the material are summarized in Table 1. Since in this problem gas pressure changes are small in comparison to atmospheric pressure, the constant bulk modulus equal to the atmospheric pressure is assumed. Indeed in this example, the values of the air compressibility varies in the range of 10^{-5} to 1.064×10^{-5} and this limited range of changes justifies this assumption. To improve accuracy, the solution domain is discretized into a fine grid with 100 nodes. Also an adaptive time

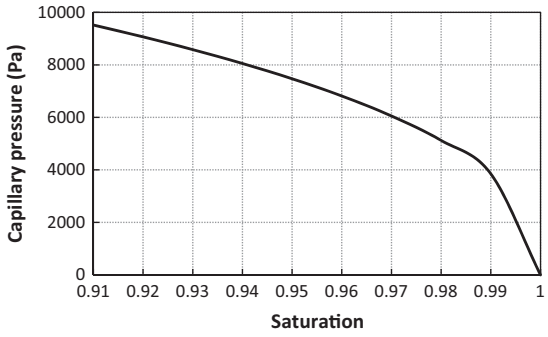

Fig. 4. Liakopoulos experiment: capillary pressure vs. water saturation (Eq. 40).

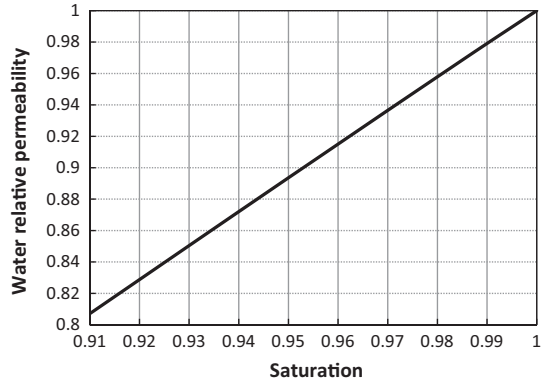

Fig. 5. Liakopoulos experiment: water relative permeability vs. water saturation (Eq. 41).

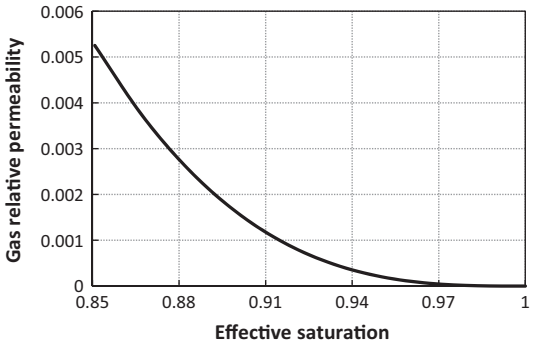

Fig. 6. Liakopoulos experiment: gas relative permeability vs. effective saturation (Eq. 42).

Table 1
Material properties of the Liakopoulos test.

Parameters	Values
Intrinsic permeability	$k = 4.5 \times 10^{-13}$ m^2
Viscosity of water	$\mu_w = 0.001$ Pa s
Viscosity of air	$\mu_g = 1.8 \times 10^{-5}$ Pa s
Solid phase density	$\rho_s = 2000$ kg/m^3
Water density	$\rho_w = 1000$ kg/m^3
Air density	$\rho_g = 1.2$ kg/m^3
Biot coefficient	$\alpha = 1.0$
Porosity	$\phi = 0.2975$
Bulk modulus of solid phase	$K_S = 1 \times 10^{12}$ Pa
Bulk modulus of water	$K_w = 2 \times 10^9$ Pa
Bulk modulus of air	$K_g = 0.1 \times 10^6$ Pa
Pore size distribution index	$\lambda = 3$
Residual water saturation	$S_{rw} = 0.2$
Young's modulus	$E = 1.3 \times 10^6$ Pa
Poisson's ratio	$\vartheta = 0.4$
Gravitational acceleration	$g = 9.81$ m/s^2
Atmospheric pressure	$p_{atm} = 0$ Pa

stepping strategy similar to that suggested in [58] was applied. According to the number of iterations, if more than 8 iterations were required for convergence at the previous time step, the next time step is reduced by 5%, while for the Picard iterations of less than 4 it is increased 5%. The time-step size of 0.5 s is assumed initially which updated automatically during the course of the computation. Run-time information of the adaptive time-stepping method for the pressure form and the modified Picard, with respect to the total number of iterations and time steps are summarized in Table 2.

In this numerical simulation, as considered in the aforementioned references, first the pressure-based formulation is used to obtain the solution. In the following figures, the gas pressure, water pressure, water saturation and vertical displacement distributions over the column height at selected times are presented. Then, the mixed form method has been tested. In this scheme, numerical oscillations occur at or near the fully saturated regions during the initial time step which result in the algorithm becoming unstable. To reach a convergent solution, the standard convergence criterion, which considered the maximum absolute difference between values of pressure, saturation and displacement of two successive iterations, with large tolerance values has been implemented. But oscillations in the values of saturation were still observed and low accurate solutions for pressure values would be obtained.

To resolve the stability problems of the mixed form, the modified Picard iteration method is applied. The simulated profiles from the modified Picard approach are compared with the results of the pressure based method as shown in Figs. 7–10. As the profiles show, both algorithms give very similar results which closely correspond to those in Refs. [7,51]. The difference between the results of the two methods remains, even by assuming a constant time step. This is mainly due to the selection of the primary variables. Since the expansion of the time derivative term is the main difference between these numerical approximations, it is the cause of these differences. Furthermore, as shown in Table 2, the modified Picard method is able to achieve accurate solutions with very large time steps, which indicates the efficiency of this method.

4.1.2. Partially saturated consolidation problem

In the second example, the model of immiscible multiphase flow has been tested in a partially saturated consolidation problem. For this purpose the results are compared with the finite element solutions which have been presented by Rahman and Lewis [6] and then by Khoei and Mohammadnejad [51]. In this problem a soil column of 1 m height is subjected to an external surface load of 1000 Pa. At the beginning a partially saturated state with water saturation of 0.52 and pore water pressure of −280 kPa is assumed, as well as a mechanical equilibrium state. At the top boundary condition the value of pore water pressure is instantaneously changed from −280 kPa to −420 kPa, while the air pressure remains constant at atmospheric pressure. The basement is fixed and no-flow boundary condition is applied at bottom for both water and air (Fig. 11. Also there is no gravity. The mechanical and hydraulic properties of the porous media are listed in Table 3. The simulations were performed by using the Brooks–Corey hydraulic functions as follows [57]:

$$S_e = \begin{cases} S_{rw} + (1 - S_{rw}).(p_c/p_d)^{-\lambda} & \text{if } p_c < p_d \\ 1 & \text{if } p_c \geqslant p_d \end{cases}$$
$$k_{rw} = S_e^{(2+3\lambda)/\lambda} \qquad (44)$$
$$k_{rg} = (1 - S_e)^2 \left(1 - S_e^{\frac{(2+\lambda)}{\lambda}}\right)$$

Table 2
Run-time information for the adaptive time-stepping method for the pressure based and modified Picard methods.

	t = 5 min	t = 10 min	t = 20 min	t = 30 min	t = 60 min	t = 120 min
Pressure based method						
NI[a]	875	1026	1240	1804	3442	5132
NTS[b]	221	273	307	376	616	851
Δt_{max}(s)	3.041	13.142	13.593	7.345	9.444	22.248
Modified Picard method						
NI	333	396	477	555	719	875
NTS	97	118	138	157	201	244
Δt_{max}(s)	8.068	22.477	31.627	31.627	56.798	123.983

[a] NI is the total number of iterations, during the simulation.
[b] NTS is the total number of timesteps, during the simulation.

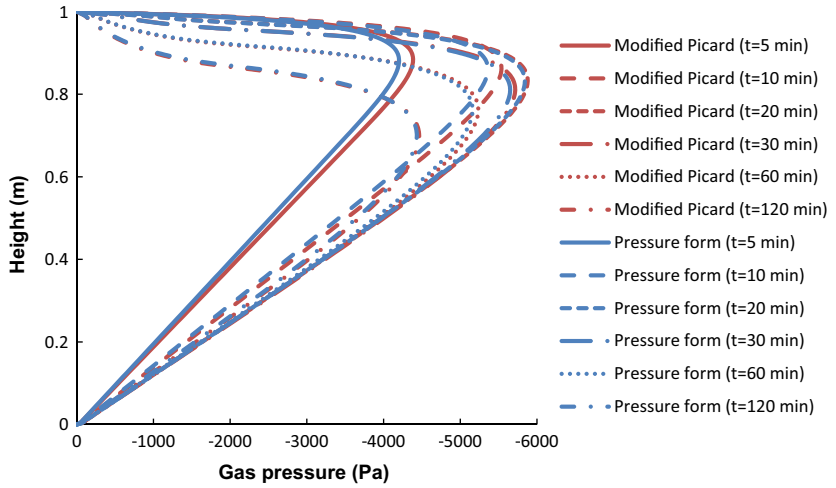

Fig. 7. Liakopoulos experiment: gas pressure profiles obtained by using the pressure form and the modified Picard scheme.

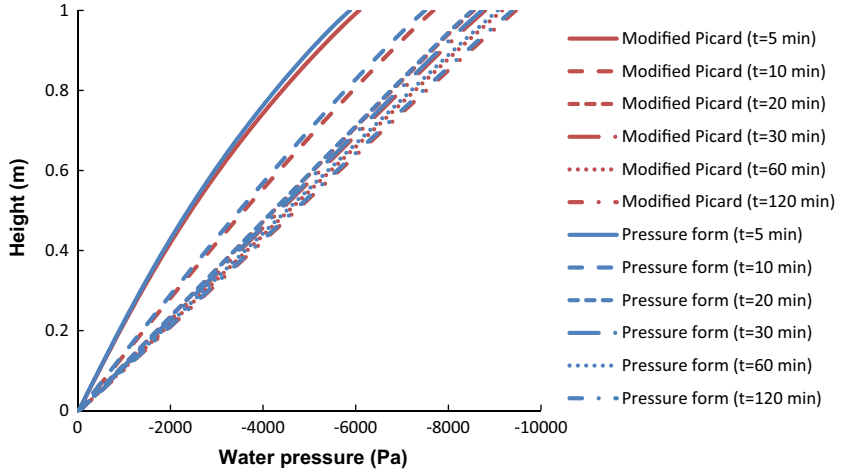

Fig. 8. Liakopoulos experiment: water pressure profiles obtained by using the pressure form and the modified Picard scheme.

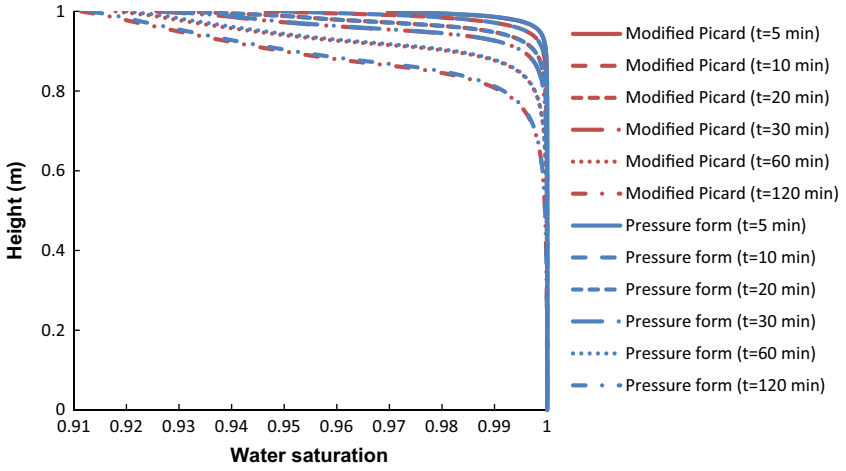

Fig. 9. Liakopoulos experiment: water saturation profiles obtained by using the pressure form and the modified Picard scheme.

in which the residual water saturation $S_{rw} = 0.3966$, the air-entry pressure $p_d = 225 \times 10^3$ Pa and λ, the pore size distribution index is 3. The number of nodes of 20 and time step of 1 s, are chosen in this simulation. The resulting profiles of water pressure, water

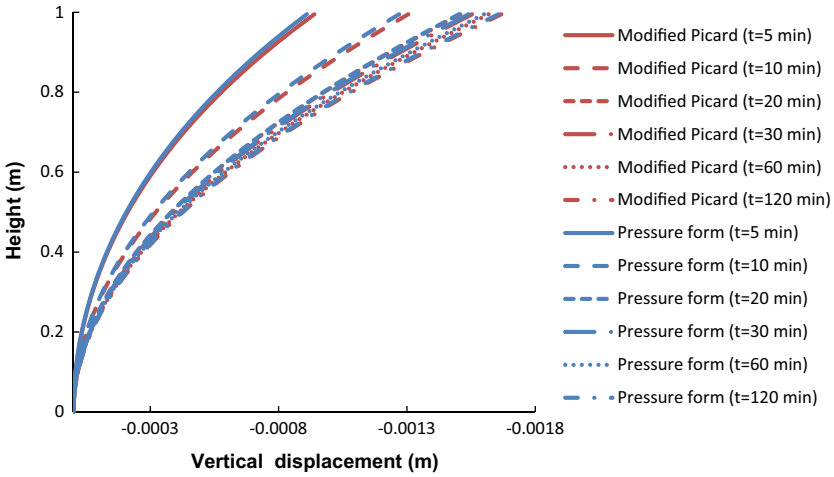

Fig. 10. Liakopoulos experiment: vertical displacement profiles obtained by using the pressure form and the modified Picard scheme.

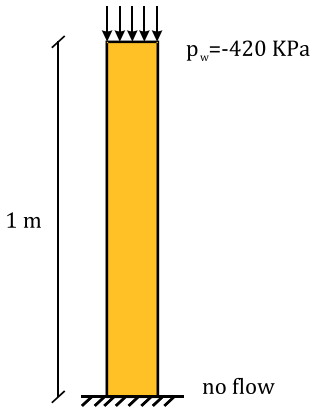

Fig. 11. Partially saturated consolidation problem: configuration of the problem with assumed boundary conditions.

Table 3
Partially saturated consolidation problem: hydraulic and mechanical parameters of the porous medium.

Parameters	Values
Intrinsic permeability	$k = 0.46 \times 10^{-11}$ m^2
Viscosity of water	$\mu_w = 0.001$ Pa s
Viscosity of air	$\mu_g = 0.001$ Pa s
Solid phase density	$\rho_s = 2000$ kg/m^3
Water density	$\rho_w = 1000$ kg/m^3
Air density	$\rho_g = 1.22$ kg/m^3
Biot coefficient	$\alpha = 1.0$
Porosity	$\phi = 0.3$
Bulk modulus of solid phase	$K_S = 0.14 \times 10^{10}$ Pa
Bulk modulus of water	$K_w = 0.43 \times 10^{13}$ Pa
Bulk modulus of air	$K_g = 0.1 \times 10^{6}$ Pa
Young's modulus	$E = 6 \times 10^{6}$ Pa
Poisson's ratio	$\vartheta = 0.4$
Atmospheric pressure	$p_{atm} = 101.325 \times 10^{3}$ Pa

saturation and vertical displacements for mixed, modified Picard and pressure forms of multiphase flow, are shown in Figs. 12–14. The profiles obtained with the FVM, for these forms of equations, show very good agreement with the results reported in Ref. [6]. These results could also be compared with the results of [51] which have solved the problem with the assumption of imposed gravity, the comparison with these references shows the negligible effect of the gravity in the final results. In this partially saturated condition all of these schemes are stable and convergent.

Despite stability and convergence properties, these schemes are evaluated in terms of mass balance error to examine acceptability and solution accuracy. The mass balance errors of the pressure form, modified Picard and the mixed form for different time steps during the simulation are summarized in Table 4. As the results show, for the pressure form, mass balance errors are about 5%. The modified Picard method and the mixed form pose very good mass balance property. In Table 4. by increasing the time step, the cumulative mass balance errors improve. This occurs because on the first time step of the simulation, there is an inconsistency between boundary and initial conditions, which might make a relatively large incremental mass balance error. This value at the first time step will increase by decreasing the time step size and affects the cumulative mass balance error during the simulation.

4.1.3. Mcwhorter and Suanda problem: Initially saturated with an incompressible non-wetting fluid

Mcwhorter and Suanda [60] have developed an exact integral solution for unsteady two phase flow, in a one-dimensional horizontal system. In this process of unidirectional displacement of oil by water, capillary pressure is considered but gravity is neglected. In order to examine the coupled solution of fluid flow and geomechanics, the porous medium is considered deformable. In this example, the mechanical properties which are applied to the poroelastic media are listed in Table 5. Other hydraulic parameters and relationships are assumed as [27,60]. As mentioned in [60], the right boundary is closed and not affected by the inflow. So it could be assumed as a non-conductive boundary. As shown in Fig. 15, the Dirichlet boundary conditions are imposed to the left boundary condition. For the mechanical problem, zero displacement is considered at both ends. In this situation the length of the specimen is fixed. The column is initially saturated with non-wetting fluid, but to avoid numerical instability, water saturation at the initial condition is assumed 0.01 as [60]. It should be mentioned that both fluid phases are considered incompressible. To consider the incompressibility of the fluids, the inverse of the bulk modulus (i.e. fluid compressibility) is set equal to zero $\frac{1}{K_f} = 0$. To implement it, the terms including bulk modulus of the fluids $\left(\frac{nS_w}{K_w}$ and $\frac{n(1-S_w)}{K_{nw}}\right)$ have been removed from the general equations. The domain is discretized into 80 control volumes and the time discretization is based on the implicit Euler method. Because of

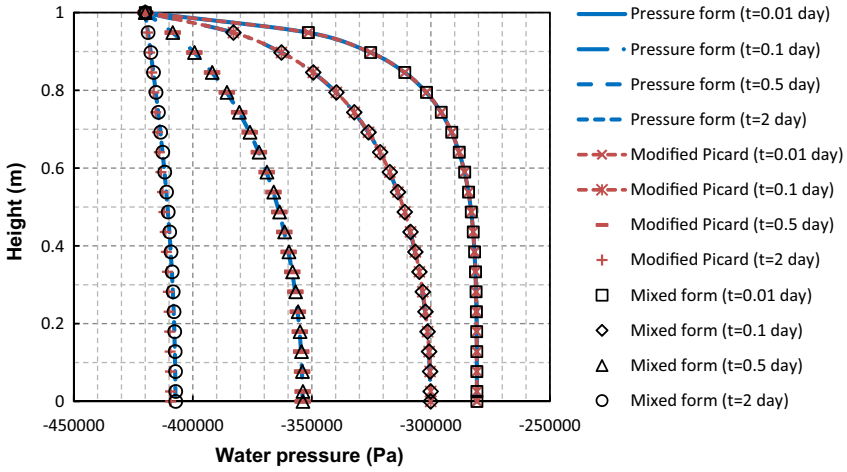

Fig. 12. Partially saturated consolidation problem: mixed, modified Picard and pressure forms of numerical solutions for the pore water pressure.

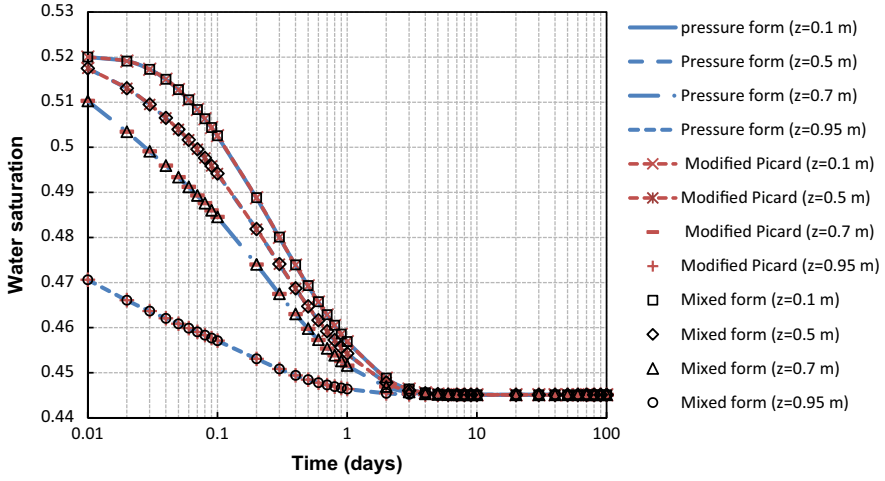

Fig. 13. Partially saturated consolidation problem: mixed, modified Picard and pressure forms of numerical solutions for water saturation.

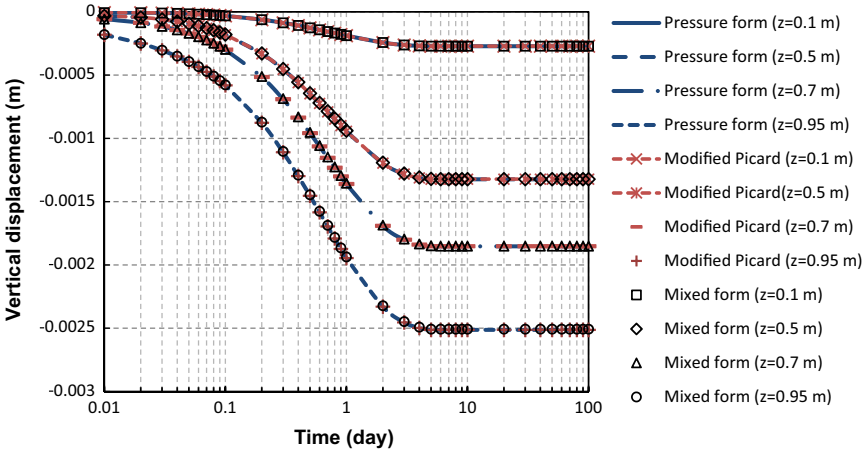

Fig. 14. Partially saturated consolidation problem: mixed, modified Picard and pressure forms of numerical solutions for the vertical displacements.

the zero-displacement boundary conditions and the poroelastic model used for this study, deformation is only caused by the pressure gradient and the resulting solutions are very smooth. In this way, the solutions of the flow equations (i.e. pressures and saturation) are not significantly affected by geomechanical deformations. So the numerical models are compared with the

Table 4
Partially saturated consolidation problem: Mass balance errors for the pressure form, modified Picard and the mixed form.

Simulation time	100 s			864 s (0.01 day)			8640 s (0.1 day)		
Time step	1 s	4 s	8 s	1 s	4 s	8 s	1 s	4 s	8 s
Pressure form	0.0553	0.0501	0.0437	0.034	0.0317	0.0293	0.0295	0.0289	0.0281
Modified Picard	0.0007	0.0007	0.0007	0.001	0.001	0.001	0.0012	0.0012	0.0012
Mixed form	0.0007	0.0007	0.0006	0.0009	0.0009	0.0009	0.0012	0.0012	0.0012

Table 5
Mcwhorter problem: hydraulic and mechanical parameters of the porous medium (test case 3).

Parameters	Values
Intrinsic permeability	$k = 10^{-10}$ m^2
Viscosity of water	$\mu_w = 0.001$ Pa s
Viscosity of oil	$\mu_{nw} = 0.001$ Pa s
Water density	$\rho_w = 1000$ kg/m^3
Oil density	$\rho_{nw} = 1000$ kg/m^3
Biot coefficient	$\alpha = 1.0$
Porosity	$\phi = 0.3$
Young's modulus	$E = 5 \times 10^6$ Pa
Poisson's ratio	$\vartheta = 0.4$
Residual water saturation	$S_{rw} = 0$
Residual oil saturation	$S_{rnw} = 0$
Entry pressure	$p_d = 5000$ Pa
Pore size distribution index	$\lambda = 2$

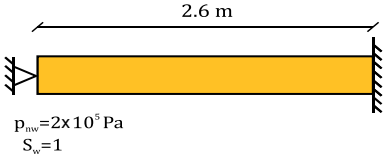

Fig. 15. Sketch of the problem setup for the Mcwhorter problem.

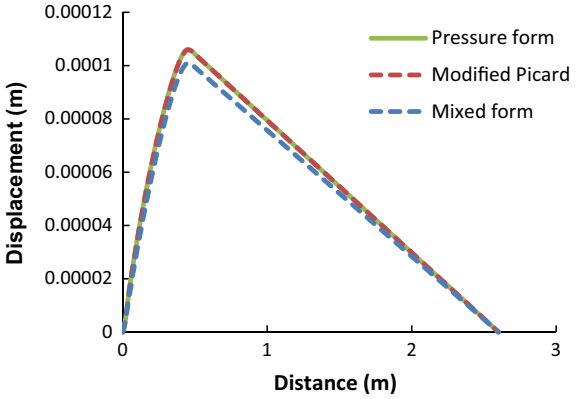

Fig. 17. Mcwhorter problem: displacement at $t = 1000$ s for pressure form, modified Picard and mixed form.

Table 6
Mcwhorter problem: water mass balance errors for the pressure form, modified Picard and the mixed form ($N = 80$).

Simulation time	100 s	500 s	1000 s	4000 s
Pressure form	0.03641	0.02102	0.01565	0.00769
Modified Picard	0.00041	0.00034	0.00012	0.00036
Mixed form	0.00048	0.0005	0.00049	0.00041

quasi-analytical solution of Ref. [60] at three selected time intervals. Fig. 16. shows accurate solutions for all forms of the discretized methods discussed above. Also for the displacement as shown in Fig. 17, the compaction and dilation occur behind and ahead of the water front, respectively.

Furthermore, in order to check the mass balance accuracy, water mass balance errors for two different mesh sizes with 80 and 20 nodes are listed in Tables 6 and 7, respectively. In Table 6, time step size varies between 0.01 s to 1 s in the first 10 s to guarantee the convergence of the solution and remains constant during the simulation. In Table 7, two time step size of 5 and 10 s are considered throughout the computation. The result indicates that for the pressure form, a small time step and a fine grid are required to obtain an accurate mass balance and for larger time steps, the mass balance error exceeded 15%. While the two other schemes yield superior mass balance results, even for large time steps and grid sizes.

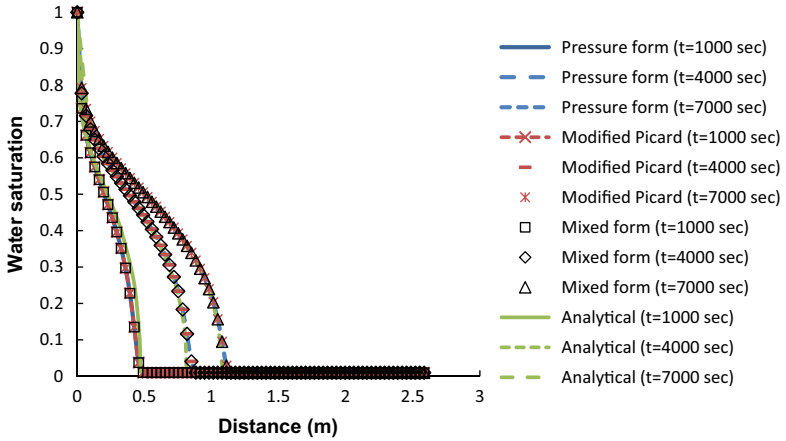

Fig. 16. Mcwhorter problem: saturation profiles at three selected times for pressure form, modified Picard, mixed form and analytical solutions.

Table 7
Mcwhorter problem: water mass balance errors for the pressure form, modified Picard and the mixed form ($N = 20$).

Simulation time	100 s		500 s		1000 s		4000 s	
Time step	5 s	10 s	5 s	10 s	5 s	10 s	5 s	10 s
Pressure form	0.1524	0.1831	0.09036	0.114	0.06975	0.08977	0.04013	0.05233
Modified Picard	0.00033	0.00035	0.0004	0.00043	0.0002	0.0004	0.0005	0.0004
Mixed form	0.00018	0.00024	0.0003	0.00031	0.00033	0.00033	0.00033	0.00034

4.1.4. Mcwhorter problem: Initially saturated with an incompressible wetting fluid

In this example, Mcwhorter problem is considered for the case in which the column is initially saturated with the wetting phase [27,59]. In this model, the oil phase infiltration through the deformable soil column with the length of 10 m has been simulated. For the left boundary condition at oil infiltration point, water saturation is equal to 0.525 and no water flow condition is prescribed. Also for the mechanical problem, the same boundary conditions are employed as in the last test case. The fluid and solid matrix properties are summarized in Table 8. The domain is subdivided into 50 control volumes and the time discretization is done with constant time step of 100 s. Fig. 18 illustrates the agreement between the numerical models and analytical solution for the distribution of fluid saturations in the column at various times for all of the three schemes.

As the previous examples, mass balance analysis has been performed for the different strategies with various mesh sizes and time steps. As a result, the maximum mass balance error for the mixed form and the modified Picard scheme is limited to 0.1%, throughout the simulation, while for the pressure form it exceeds 5%.

Table 8
Mcwhorter problem: hydraulic and mechanical parameters of the porous medium (test case 4).

Parameters	Values
Intrinsic permeability	$k = 5 \times 10^{-11}$ m^2
Viscosity of water	$\mu_w = 0.001$ Pa s
Viscosity of oil	$\mu_{nw} = 0.0005$ Pa s
Water density	$\rho_w = 1000$ kg/m^3
Oil density	$\rho_{nw} = 1000$ kg/m^3
Biot coefficient	$\alpha = 1.0$
Porosity	$\phi = 0.35$
Young's modulus	$E = 5 \times 10^6$ Pa
Poisson's ratio	$\vartheta = 0.4$
Residual water saturation	$S_{rw} = 0.05$
Residual oil saturation	$S_{rnw} = 0.05$
Entry pressure	$p_d = 2000$ Pa
Pore size distribution index	$\lambda = 2$

4.2. Comparison of the coupling schemes

In this section the fixed-stress algorithm has been implemented to the finite volume simulator for the different forms of the equations. Accuracy, rate of convergence and efficiency of this iteratively coupled method have been investigated. For this purpose, two kinds of boundary conditions have been considered for the mechanical equation. First is the boundary condition in which the vertical load is constant. According to this assumption and under uniaxial strain condition, the volumetric strain is equal to the vertical strain and can be obtained in terms of the average pore pressure from the mechanical equation. For the boundary condition type 2, vertical displacement is imposed on both ends of the geomechanical domain. In this kind of boundary condition the vertical stress is calculated from the boundary values of the displacement and the pressure variation through the domain [54]. The first and second test cases in this study including Liakopoulos [7,51] drainage test and the partially saturated consolidation problem [6,51], have been simulated using a boundary condition type one due to the prescribed vertical traction. While, in both Mcwhorter problems [59], boundary condition type 2 (constant vertical displacement) is assumed and imposed. To perform comparative analysis between coupling schemes, the partially saturated consolidation problem and the Mcwhorter problem (Initially saturated

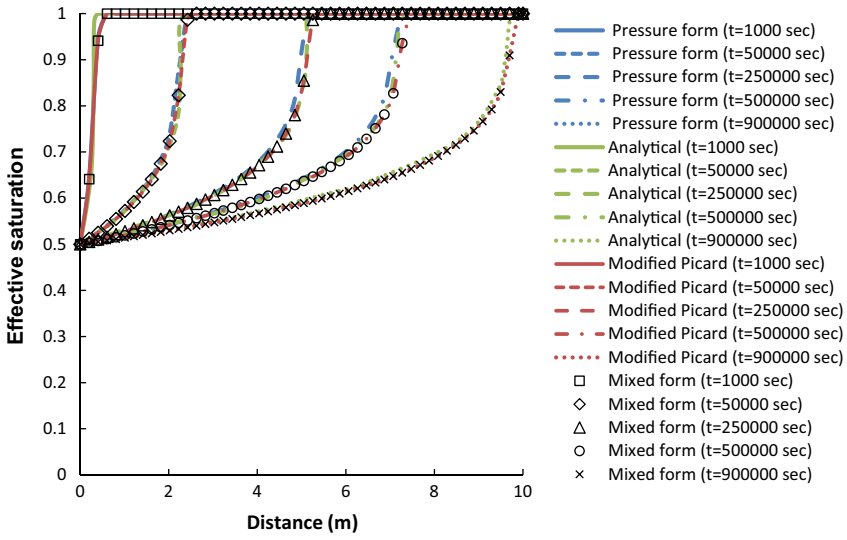

Fig. 18. Mcwhorter problem: effective saturation profiles at selected times for pressure form, modified Picard, mixed form and analytical solutions.

Table 9
Run-time information for boundary condition type 1.

Comparison factors	Iteratively coupled method			Fully coupled method		
	Pressure form	Modified Picard	Mixed form	Pressure form	Modified Picard	Mixed form
Total iteration	86,894	86,899	87,202	91,036	91,035	87,244
CPU Time (s)	407.76	461.62	472.30	1127.55	1124.28	1097.83

Table 10
RMSE for boundary condition type 1.

Comparison factors	Iteratively coupled method		
	Pressure form	Modified Picard	Mixed form
RMSE-p_w (Pa)	0.3688	4.6203	0.6041
RMSE-p_{nw} (Pa)	0.0007	0.0088	0.0012
RMSE-S_w	2.57E−07	3.2E−06	4.2E−07
RMSE-u (m)	6.15E−09	3.98E−08	7.551E−09

with the non-wetting phase) are used for the boundary conditions type 1 and 2, respectively.

4.2.1. Boundary condition type 1: Partially saturated consolidation problem

The run-time information and accuracy of the results for the pressure form, mixed form and mixed form with a modified Picard linearization are presented in Tables 9 and 10, respectively. For the results listed in these two tables, simulations have been performed with a time step of 0.1 s, with 80 control volumes and at time $t = 0.1$ day. The number of total iterations of the iteratively coupled method, for all of the numerical schemes are fewer than the fully coupled method. Since, the fixed-stress split supposes that the rate of the volumetric stress is constant during the flow step, for the boundary condition type 1, this restriction is satisfied automatically. So, the problem converges with less iteration numbers than the fully coupled method. As a consequence, CPU time decreases significantly due to the less number of iterations and the matrices with smaller dimensions.

In Table 10, root mean square errors (RMSE) of the pressures, saturation and displacement values are calculated to compare the sequential methods with the fully coupled solution. As the results indicate, all of the numerical models are very accurate.

4.2.2. Boundary condition type 2: Mcwhorter problem (Initially saturated with the non-wetting phase)

In the following simulations, results are obtained at $t = 1000$ s, with a time step which varies between 0.01 s to 1 s in the first 10 s and then remains constant. Also 80 nodes are considered for spatial discretization. As shown in Table 11, the iteratively coupled methods required less number of iterations to converge, in all of the cases. The resulting large sparse and ill-posed matrix obtained from the fully coupled method incurs higher computational cost especially in terms of CPU time. The values of RMSE in Table 12, show that the iteratively coupled solution predicts the same result as the fully coupled method and retains accuracy for all of the numerical methods.

Table 12
RMSE for boundary condition type 2.

Comparison factors	Iteratively coupled method		
	Pressure form	Modified Picard	Mixed form
RMSE-p_w (Pa)	2.944494	4.61742	26.25074
RMSE-p_{nw} (Pa)	1.343311	1.45464	3.225233
RMSE-S_w	1.49742E−05	1.51276E−05	0.000187
RMSE-u (m)	3.35283E−06	2.50173E−06	7.19263E−07

5. Conclusions

In this study, three forms of the coupled multiphase flow and geomechanics including pressure form, mixed form and mixed form with a modified Picard linearization are developed and assessed. A finite volume method is used to enforce local conservation for discretization of the governing equations. Although, these forms of equations are mathematically equivalent, they lead to different numerical results. Therefore, these models have been studied according to the different aspects such as stability, convergence and mass conservation. The mass conservation is the issue which has not been investigated in the case of the deformable porous media. The proposed models are verified against different examples. Also, an iterative coupling technique based on fixed-stress algorithm is employed to solve the coupled equations. The fully coupled and the iteratively coupled methods have been compared with two types of boundary conditions for the mechanical equation. From these test cases, the following conclusions can be drawn:

- The choice of water degree of saturation in the mixed form, as a primary variable leading to convergence problems in transition from saturated to unsaturated regimes. The pressure form and the mixed form with a modified Picard linearization show good convergence even near the fully saturated conditions.
- Despite the pressure form has been widely used in the geotechnical engineering, it provides poor mass balance, while the two other methods exhibited excellent mass balance accuracy over any spatiotemporal mesh in all of the test cases.
- A comparison analysis for the fixed-stress split as an iteratively coupled method demonstrated the accuracy, robustness and efficiency of this method due to the reduced CPU time and low values of RMSE. So this method is also highly recommended in the case of multiphase fluid.

Table 11
Run-time information for boundary condition type 2.

Comparison factors	Iteratively coupled method			Fully coupled method		
	Pressure form	Modified Picard	Mixed form	Pressure form	Modified Picard	Mixed form
Total iteration	2067	2045	3158	2068	2048	3176
CPU time (s)	6.28	6.22	10.00	41.5	39.12	63.16

Acknowledgments

The authors wish to thank the Editor-in-Chief Professor Hywel R. Thomas and also three anonymous reviewers for their constructive comments which helped to improve the final manuscript.

References

[1] Zobach MD. Reservoir geomechanics. Cambridge Press; 2010.
[2] Ataie-Ashtiani B, Hassanizadeh SM, Oostrom M, Celia MA, White MD. Effective parameters for two-phase flow in a porous medium with periodic heterogeneities. J Contam Hydrol 2001;49(1):87–109.
[3] Ataie-Ashtiani B, Hassanizadeh SM, Celia MA. Effects of heterogeneities on capillary pressure–saturation–relative permeability relationships. J Contam Hydrol 2002;56(3):175–92.
[4] Ataie-Ashtiani B, Hassanizadeh SM, Oung O, Weststrate FA, Bezuijen A. Numerical modelling of two-phase flow in a geocentrifuge. Environ Modell Softw 2003;18(3):231–41.
[5] Bear J, Cheng AD. Modeling groundwater flow and contaminant transport, vol. 23. Springer; 2010.
[6] Rahman NA, Lewis RW. Finite element modelling of multiphase immiscible flow in deforming porous media for subsurface systems. Comput Geotech 1999;24(1):41–63.
[7] Lewis RW, Schrefler BA. The finite element method in the static and dynamic deformation and consolidation of porous media. 2nd ed. Chichester: Wiley; 1998.
[8] Zienkiewicz OC, Chan AHC, Pastor M, Schrefler BA, Shiomi T. Computational geomechanics with special reference to earthquake engineering. NewYork: Wiley; 1999.
[9] Schrefler BA, Xiaoyong Z. A fully coupled model for water flow and airflow in deformable porous media. Water Resour Res 1993;29(1):155–67.
[10] Kolditz O. Computational methods in environmental fluid mechanics. Springer; 2002.
[11] Kihm JH, Kim JM, Song SH, Lee GS. Three-dimensional numerical simulation of fully coupled groundwater flow and land deformation due to groundwater pumping in an unsaturated fluvial aquifer system. J Hydrol 2007;335(1):1–14.
[12] Forsyth PA, Unger AJA, Sudicky EA. Nonlinear iteration methods for nonequilibrium multiphase subsurface flow. Adv Water Resour 1998;21(6):433–49.
[13] Sanavia L, Pesavento F, Schrefler BA. Finite element analysis of non-isothermal multiphase geomaterials with application to strain localization simulation. Comput Mech 2006;37(4):331–48.
[14] Celia MA, Binning P. A mass conservative numerical solution for two-phase flow in porous media with application to unsaturated flow. Water Resour Res 1992;28(10):2819–28.
[15] Li X. Finite-element analysis for immiscible two-phase fluid flow in deforming porous media and an unconditionally stable staggered solution. Commun Appl Numer M 1990;6(2):125–35.
[16] Li X, Zienkiewicz OC, Xie YM. A numerical model for immiscible two-phase fluid flow in a porous medium and its time domain solution. Int J Numer Meth Eng 1990;30(6):1195–212.
[17] Yang D, Moridis GJ, Blasingame TA. A fully coupled multiphase flow and geomechanics solver for highly heterogeneous porous media. J Comput Appl Math 2014;270:417–32.
[18] Schrefler BA, Zhan X, Simoni L. A coupled model for water flow, airflow and heat flow in deformable porous media. Int J Numer Method H 1995;5(6):531–47.
[19] Laloui L, Klubertanz G, Vulliet L. Solid–liquid–air coupling in multiphase porous media. Int J Numer Anal Methods Geomech 2003;27(3):183–206.
[20] Schrefler BA, Scotta R. A fully coupled dynamic model for two-phase fluid flow in deformable porous media. Comput Methods Appl Mech Eng 2001;190(24):3223–46.
[21] Kolditz O, Bauer S, Böttcher N, Elsworth D, Görke UJ, McDermott CI, et al. Numerical simulation of two-phase flow in deformable porous media: application to carbon dioxide storage in the subsurface. Math Comput Simulat 2012;82(10):1919–35.
[22] Gawin D, Baggio P, Schrefler BA. Coupled heat, water and gas flow in deformable porous media. Int J Numer Methods Fluids 1995;20:969–87.
[23] Gawin D, Schrefler BA. Thermo-hydro-mechanical analysis of partially saturated porous materials. Eng Comput 1996;13(7):113–43.
[24] Celia MA, Bouloutas ET, Zarba RL. A general mass-conservative numerical solution for the unsaturated flow equation. Water Resour Res 1990;26(7):1483–96.
[25] Lehmann F, Ackerer PH. Comparison of iterative methods for improved solutions of the fluid flow equation in partially saturated porous media. Transport Porous Med 1998;31(3):275–92.
[26] Abriola LM, Rathfelder K. Mass balance errors in modeling two-phase immiscible flows: causes and remedies. Adv Water Resour 1993;16(4):223–39.
[27] Ataie-Ashtiani B, Raeesi-Ardekani D. Comparison of numerical formulations for two-phase flow in porous media. Geotech Geol Eng 2010;28(4):373–89.
[28] Shahraiyni HT, Ataie-Ashtiani B. Mathematical forms and numerical schemes for the solution of unsaturated flow equations. J Irrig Drain E-ASCE 2011;138(1):63–72.
[29] Wan J. Stabilized finite element methods for coupled geomechanics and multiphase flow. PhD dissertation. Stanford University; 2002.
[30] Lewis RW, Sukirman Y. Finite element modelling of three-phase flow in deforming saturated oil reservoirs. Int J Numer Anal Methods Geomech 1993;17(8):577–98.
[31] Kim J, Tchelepi HA, Juanes R. Rigorous coupling of geomechanics and multiphase flow with strong capillarity. SPE J 2013;18(06).
[32] Vermeer PA, Verruijt A. An accuracy condition for consolidation by finite elements. Int J Numer Anal Methods Geomech 1981;5(1):1–14.
[33] Murad MA, Loula AFD. Improved accuracy in finite element analysis of Biot's consolidation problem. Comput Methods Appl Mech Eng 1992;95(3):359–82.
[34] Murad MA, Loula AFD. On stability and convergence of finite element approximations of Biot's consolidation problem. Int J Numer Methods Eng 1994;37(4):645–67.
[35] Asadi R, Ataie-Ashtiani B, Simmons CT. Finite volume coupling strategies for the solution of a Biot consolidation model. Comput Geotech 2014;55:494–505.
[36] Caviedes-Voullième D, Garcı'a-Navarro P, Murillo J. Verification, conservation, stability and efficiency of a finite volume method for the 1D Richards equation. J Hydrol 2013;480:69–84.
[37] Szymkiewicz A, Helmig R. Comparison of conductivity averaging methods for one-dimensional unsaturated flow in layered soils. Adv Water Resour 2011;34(8):1012–25.
[38] Settari A, Walters DA. Advances in coupled geomechanical and reservoir modeling with applications to reservoir compaction. SPE J 2001;6(03):334–42.
[39] Dean RH, Gai X, Stone CM, Minkoff SE. A comparison of techniques for coupling porous flow and geomechanics. SPE J 2006;11(1):132–40.
[40] Settari A, Mourits FM. A coupled reservoir and geomechanical simulation system. SPE J 1998;3(3):219–26.
[41] Gutierrez M, Lewis RW. The role of geomechanics in reservoir simulation. In: EUROCK 98. Symposium; July 1998.
[42] Chin LY, Thomas LK. Fully coupled analysis of improved oil recovery by reservoir compaction. In: SPE annual technical conference; October 1999.
[43] Huang H, Wattenbarger R, Gai X, Brown WP, Hehmeyer OJ, Wang J, et al. Using a fully coupled flow and geomechanical simulator to model injection into heavy oil reservoirs. Int J Numer Meth Fl 2013;71(6):671–86.
[44] Pao WKS, Lewis RW, Masters I. A fully coupled hydro-thermo-poro-mechanical model for black oil reservoir simulation. Int J Numer Anal Meth Geomech 2001;25(12):1229–56.
[45] Zhao N. Integration of reservoir simulation and geomechanics. PhD dissertation. The University of Utah; 2012.
[46] Kim J, Tchelepi HA, Juanes R. Stability, accuracy, and efficiency of sequential methods for coupled flow and geomechanics. SPE J 2011;16(2):249–62.
[47] Kim J, Tchelepi H, Juanes R. Stability and convergence of sequential methods for coupled flow and geomechanics: drained and undrained splits. Comput Methods Appl Mech Eng 2011;200(23):2094–116.
[48] Kim J, Tchelepi H, Juanes R. Stability and convergence of sequential methods for coupled flow and geomechanics: fixed-stress and fixed-strain splits. Comput Methods Appl Mech Eng 2011;200(13):1591–606.
[49] Gaspar FJ, Lisbona FJ, Vabishchevich PN. Staggered grid discretizations for the quasi-static Biot's consolidation problem. Appl Numer Math 2006;56(6):888–98.
[50] Naumovich A, Gaspar FJ. On a multigrid solver for the three-dimensional Biot poroelasticity system in multilayered domains. Comput Vis Sci 2008;11(2):77–87.
[51] Khoei AR, Mohammadnejad T. Numerical modeling of multiphase fluid flow in deforming porous media: a comparison between two-and three-phase models for seismic analysis of earth and rockfill dams. Comput Geotech 2011;38(2):142–66.
[52] Huang K, Mohanty BP, van Genuchten MTh. A new convergence criterion for the modified Picard iteration method to solve the variably saturated flow equation. J Hydrol 1996;178(1):69–91.
[53] Kaluarachchi JJ, Parker JC. An efficient finite element method for modeling multiphase flow. Water Resour Res 1989;25(1):43–54.
[54] Jeannin L, Mainguy M, Masson R, Vidal-Gilbert S. Accelerating the convergence of coupled geomechanical-reservoir simulations. Int J Numer Anal Methods Geomech 2007;31(10):1163–81.
[55] Kim J. Sequential methods for coupled geomechanics and multiphase flow. Phd thesis. Stanford University; 2010.
[56] Liakopoulos AC. Transient flow through unsaturated porous media. PhD thesis. Berkeley (CA): University of California; 1965.
[57] Brooks RN, Corey AT. Properties of porous media affecting fluid flow. J Irrigat Drain Div Am Soc Civil Eng 1966;92:61–88.
[58] Sadegh Zadeh K. A mass-conservative switching algorithm for modeling fluid flow in variably saturated porous media. J Comput Phys 2011;230(3):664–79.
[59] McWhorter DB, Sunada DK. Exact integral solutions for two-phase flow. Water Resour Res 1990;26(3):399–414.
[60] Helmig R. Multiphase flow and transport processes in the subsurface: a contribution to the modeling of hydrosystems. Springer-Verlag; 1997.